

Fully Comprehensive Geometrically Non-Linear Dynamic Analysis of Multi-Body Beam Systems with Elastic Couplings

Hemaraju Pollayi^{1*}, Dineshkumar Harursamath²

¹ Research Scholar

² Assistant Professor

Nonlinear Multifunctional Composites Analysis and Design Lab (NMCAD Lab)

Department of Aerospace Engineering

Indian Institute of Science - Bangalore

Bangalore - 560 012, Karnataka, INDIA

* Corresponding author (email: raju@aero.iisc.ernet.in)

Abstract

This paper is concerned with the dynamic analysis of flexible, non-linear multi-body beam systems. The focus is on problems where the strains within each elastic body (beam) remain small. Based on geometrically non-linear elasticity theory, the non-linear 3-D beam problem splits into either a linear or non-linear 2-D analysis of the beam cross-section and a non-linear 1-D analysis along the beam reference line. The splitting of the three-dimensional beam problem into two- and one-dimensional parts, called dimensional reduction, results in a tremendous savings of computational effort relative to the cost of three-dimensional finite element analysis, the only alternative for realistic beams. The analysis of beam-like structures made of laminated composite materials requires a much more complicated methodology. Hence, the analysis procedure based on Variational Asymptotic Method (VAM), a tool to carry out the dimensional reduction, is used here.

The analysis methodology can be viewed as a 3-step procedure. First, the sectional properties of beams made of composite materials are determined either based on an asymptotic procedure that involves a 2-D finite element non-linear analysis of the beam cross-section to capture trapeze effect or using strip-like beam analysis, starting from Classical Laminated Shell Theory (CLST). Second, the dynamic response of non-linear, flexible multi-body beam systems is simulated within the framework of energy-preserving and energy-decaying time integration schemes that provide unconditional stability for non-linear beam systems. Finally, local 3-D responses in the beams are recovered, based on the 1-D responses predicted in the second step. Numerical examples are presented and results from this analysis are compared with those available in the literature.

Keywords: comprehensive, geometrically non-linear, VAM, flexible multi-body beam systems, and unconditional stability

1 Introduction

This paper is concerned with the dynamic analysis of flexible, non-linear multi-body systems, *i.e.* a collection of bodies in arbitrary motion with respect to each other while each body is undergoing large displacements and rotations with respect to a body attached frame of reference. The focus is on problems where the strains [1] within each elastic body remain small.

Typical beam analyses used in multi-body formulations rarely account for such basic effects as the shear center being offset from the sectional center of mass. The analysis of beam-like structures made of laminated composite materials requires a much more complicated methodology. Because of this complexity, it is common to find treatments of simple cross-sectional shapes (strips, box-beams, I-beams, etc.) as pointed in a review article by Hodges [2]. In the work of Berdichevsky [3], the three-dimensional elasticity representation of a beam was shown to give rise to two separate problems: *a linear two-dimensional problem over the beam cross-section*, which provides a set of elastic constants (elements of linear stiffness matrix) and a set of “recovering relations” for three-dimensional displacements, strain, and stress; and *a non-linear one-dimensional problem along the beam reference line*.

An extension of this methodology to generally anisotropic and inhomogeneous beams was undertaken by Cesnik and Hodges [4]. For the analysis of arbitrary beams (excluding those with thin-walled, open cross-sections) made of laminated, composite materials, a fully populated 4×4 matrix of elastic constants is found in the analysis of [4]. This linear cross-sectional analysis was generalized by Wenbin Yu [5].

Cross-sectional analyses are usually linear, but there are at least a couple of exceptions. Harursamath and Hodges [6, 7, 8] studied the bending of thin-walled, hollow, circular tubes, which leads to a non-linear moment-curvature relation. More commonly studied is the trapeze effect, a non-linear effect, which is typically included in the analyses

of rotating structures such as helicopter rotor blades, propellers, and turbomachinery blades because of the presence of large centrifugal forces. It leads to an effective torsional rigidity that varies with axial force. The trapeze effect is caused by non-linear extension-twist coupling in beams undergoing large axial forces and is caused by the presence of certain non-linear terms in the strain field because of moderate local rotation (Chapter 3 of [9]).

The equations of motion resulting from the modeling of multi-body systems present distinguishing features: they are *stiff, non-linear, differential-algebraic equations*. The stiffness of the system stems from the presence of high frequencies in the elastic members, but also from the infinite frequencies associated with the kinematic constraints. The dynamic response of non-linear, flexible multi-body beam systems is simulated within the framework of energy-preserving and energy-decaying time integration schemes [10, 11, 12, 13] that provide unconditional stability for non-linear systems. The local three-dimensional stresses in the beams are recovered based on the stress resultants predicted in the non-linear analysis over the beam cross-section.

2 Comprehensive Non-Linear Dynamic Analysis of Multi-Body Composite Beam Systems

To analyse the composite beam completely using VAM, one has to perform a fully non-linear analysis to get the 3-D response of the beam. This work is based on geometrically non-linear theory assuming the material linearity. Early analyses of anisotropic beams are using the linear stiffness matrix, output from the linear cross-sectional analysis. This is the input to the 1-D non-linear analysis codes to get the final non-linear response of the beam and it is compared with the results of 3-D finite element analyses (FEA). From this one don't get the fully non-linear solution, which is an *ad hoc* assumption. In the present analysis, without any *ad hoc* assumptions one can get the fully non-linear 3-D response of the beam and these results can be compared with the existing 3-D FEA results.

This complete analysis is a three-step procedure. First, one has to perform non-linear cross-sectional analysis keeping all 1-D strain measures equal to zero and get the stiffness matrix. Second, input this stiffness matrix to the 1-D code and perform 1-D non-linear analysis. Update this stiffness matrix and input the updated one and repeat the process till the 1-D strain measures converges and run 1-D code for final 1-D responses. Third, local 3-D responses in the beams are recovered, based on the 1-D responses predicted in the second step. The complete analysis formulation is described as below with some formulae for completeness. The basic steps of the present approach is illustrated in Fig. (1).

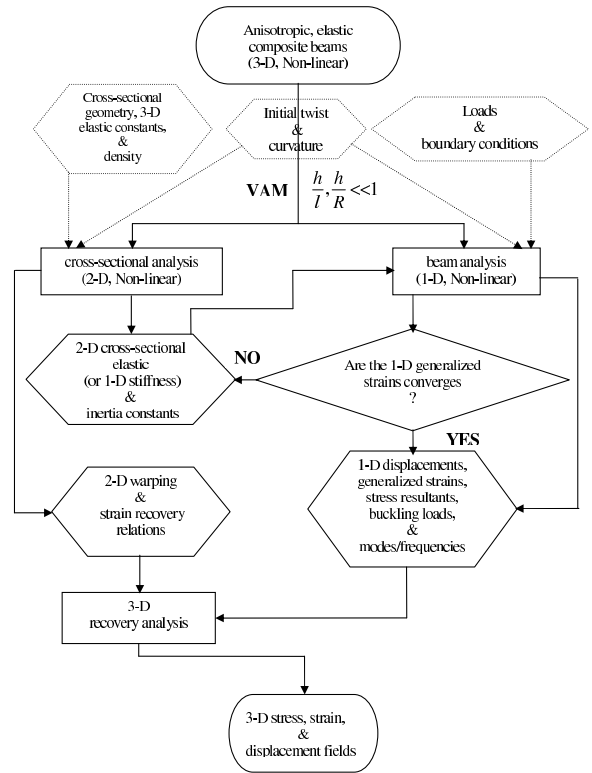


Figure 1: Flow-chart of Variational Asymptotic Analysis of Composite Beam Systems

2.1 Non-Linear 2-D Analysis of the Beam Cross-section

The non-linear 2-D analysis of the beam cross-section can be done in two-different ways using VAM. First, using the Finite Element Analysis (FEA) code Variational Asymptotic Beam Sectional Analysis (VABS) for trapeze effect and then compute the non-linear stiffness matrix. Second, the strip-beam analysis starting from Classical Laminated Shell Theory (CLST) and then compute the non-linear stiffness matrix. The presented results are based on the first approach and is described below with some necessary equations for completeness.

2.1.1 Using Finite Element code VABS

The purpose of the non-linear analysis of the beam cross-section is to determine the elements of the non-linear stiffness matrix S^{NL} and the recovering relations. The non-linear beam cross-sectional stiffness matrix, S^{NL} , relates the cross-sectional stress resultants \underline{f}^* to the generalized strain measures \underline{e}^* , a 1-D constitutive law. Recovering relations provide the relationship between the strain tensor components and the generalized strain measures \underline{e}^* . In the present notation, the 1-D constitutive law can be written as

$$\underline{f}^* = S^{NL} \underline{e}^* \quad (1)$$

where $f^* = [F_1 F_2 F_3 M_1 M_2 M_3]^T$ with F_1 as the axial force, F_2 and F_3 as transverse shear forces, M_1 as the twisting moment, M_2 and M_3 as the bending moments; $\underline{\epsilon}^* = [\gamma_{11} 2\gamma_{12} 2\gamma_{13} \kappa_1 \kappa_2 \kappa_3]^T$ with γ_{11} as the axial stretching measure of the beam, $2\gamma_{12}$ and $2\gamma_{13}$ as transverse shear measures, κ_1 as the elastic twist per unit length, κ_2 and κ_3 as elastic components of the curvature.

The 3-D strain energy density or the strain energy per unit volume

$$u_{3D} = \frac{1}{2} \Gamma^T \mathcal{D} \Gamma \quad (2)$$

This 3-D strain energy density implies a stress-strain law of the form

$$\sigma = \mathcal{D} \Gamma \quad (3)$$

where $\sigma = [\sigma_{11} \sigma_{12} \sigma_{13} \sigma_{22} \sigma_{23} \sigma_{33}]^T$ is the 3-D stress vector and $\Gamma = \Gamma(x_1, x_2, x_3) = [\Gamma_{11} 2\Gamma_{12} 2\Gamma_{13} \Gamma_{22} 2\Gamma_{23} \Gamma_{33}]^T$ is the non-linear 3-D strain vector, \mathcal{D} is the 6×6 symmetric material matrix in the oblique cross-sectional system and x_1 is the Cartesian coordinate along the axis of a beam and $x_\alpha (\alpha=2,3)$ are the Cartesian coordinates for a cross-section. Now the strain energy of the beam cross-section or the 1-D strain energy density or the strain energy per unit length or the strain energy density of the beam

$$u_{1D} = \langle u_{3D} \rangle = \frac{1}{2} \langle \Gamma^T \mathcal{D} \Gamma \rangle \quad (4)$$

and the notation $\langle \bullet \rangle \equiv \int_s \bullet \sqrt{g} dx_2 dx_3$ is used throughout the formulations for oblique cross-sectional analysis, g is the determinant of the metric tensor of the undeformed geometry with $\sqrt{g} = \beta_{11} - x_2 k_3 + x_3 k_2$ where $\beta_{ij} (i, j=1, 2, 3)$ is the direction cosine matrix of the oblique cross-section with $\beta_\alpha = \sin^{-1}(\beta_{1\alpha})$ ($\alpha=2,3$) and $\beta_{11}^2 + \beta_{22}^2 + \beta_{33}^2 = 1$, $k_\alpha (\alpha=2,3)$ are the components of the curvature of the reference line and here s is the domain stretched by undeformed cross-section.

Then the strain energy functional, u_{1D} , modified to include the ‘‘trapeze effect’’ terms, also contains third-order terms in the generalized strains. The general form is

$$u_{1D} = \frac{1}{2} \begin{Bmatrix} \gamma_{11} \\ 2\gamma_{12} \\ 2\gamma_{13} \\ \kappa_1 \\ \kappa_2 \\ \kappa_3 \end{Bmatrix}^T \begin{bmatrix} S_{11} & S_{12} & S_{13} & S_{14} & S_{15} & S_{16} \\ S_{12} & S_{22} & S_{23} & S_{24} & S_{25} & S_{26} \\ S_{13} & S_{23} & S_{33} & S_{34} & S_{35} & S_{36} \\ S_{14} & S_{24} & S_{34} & S_{44} & S_{45} & S_{46} \\ S_{15} & S_{25} & S_{35} & S_{45} & S_{55} & S_{56} \\ S_{16} & S_{26} & S_{36} & S_{46} & S_{56} & S_{66} \end{bmatrix} \begin{Bmatrix} \gamma_{11} \\ 2\gamma_{12} \\ 2\gamma_{13} \\ \kappa_1 \\ \kappa_2 \\ \kappa_3 \end{Bmatrix} + \begin{Bmatrix} \gamma_{11} \\ \kappa_1 \\ \kappa_2 \\ \kappa_3 \end{Bmatrix}^T (\gamma_{11} A_{\gamma_{11}} + \kappa_1 B_{\kappa_1} + \kappa_2 C_{\kappa_2} + \kappa_3 D_{\kappa_3}) \begin{Bmatrix} \gamma_{11} \\ \kappa_1 \\ \kappa_2 \\ \kappa_3 \end{Bmatrix} \quad (5)$$

where $A_{\bar{\gamma}_{11}}, B_{\bar{\kappa}_1}, C_{\bar{\kappa}_2}, D_{\bar{\kappa}_3}$ and $A_{\gamma_{11}}, B_{\kappa_1}, C_{\kappa_2}, D_{\kappa_3}$ are 4×4 non-classical stiffness matrices. Finally, the column matrices for 1-D strains, the non-linear 1-D strains and the warping are given by

$$\bar{\epsilon} = [\bar{\gamma}_{11} \bar{\kappa}_1 \bar{\kappa}_2 \bar{\kappa}_3]^T$$

$$\epsilon = [\gamma_{11} \kappa_1 \kappa_2 \kappa_3]^T$$

$$\bar{\epsilon}_{NL} = [\bar{\gamma}_{11}^2 \bar{\kappa}_1^2 \bar{\kappa}_2^2 \bar{\kappa}_3^2 \bar{\gamma}_{11}\bar{\kappa}_2 \bar{\gamma}_{11}\bar{\kappa}_3 \bar{\kappa}_2\bar{\kappa}_3]^T$$

$$\epsilon_{NL} = [\gamma_{11}^2 \kappa_1^2 \kappa_2^2 \kappa_3^2 \gamma_{11}\kappa_2 \gamma_{11}\kappa_3 \kappa_2\kappa_3]^T$$

$$w = [w_1 w_2 w_3]^T \quad (6)$$

Here the barred quantities $\bar{\gamma}_{11}, \bar{\kappa}_1, \bar{\kappa}_2$ and $\bar{\kappa}_3$ relate to their unbarred counterparts as

$$\overline{(\bullet)} = (\bullet)|_{2\gamma_{12}=2\gamma_{13}=0} \quad (7)$$

The cross-sectional stiffness matrix is obtained by expressing the resultant forces on the beam cross-section as

$$R \triangleq \begin{Bmatrix} F_1 \\ F_2 \\ F_3 \\ M_1 \\ M_2 \\ M_3 \end{Bmatrix} = \begin{Bmatrix} \frac{\partial u_{1D}}{\partial \gamma_{11}} \\ \frac{1}{2} \frac{\partial u_{1D}}{\partial \gamma_{12}} \\ \frac{1}{2} \frac{\partial u_{1D}}{\partial \gamma_{13}} \\ \frac{\partial u_{1D}}{\partial \kappa_1} \\ \frac{\partial u_{1D}}{\partial \kappa_2} \\ \frac{\partial u_{1D}}{\partial \kappa_3} \end{Bmatrix} \quad (8)$$

This is the most general form of the cross-sectional analysis for class \mathcal{S} and class \mathcal{T} beams.

2.2 Non-Linear 1-D Beam(s) Analysis

Beams can be defined as elastic bodies whose volume is that spanned by a cross-section translating along a smooth reference line. The beam is divided into line elements and geometrically-exact non-linear beam theory, based on mixed variational formulation, is used to perform the analysis. Combine and perform these two-analyses, non-linear 2-D cross-sectional analysis and non-linear 1-D beam analysis along the beam reference line, gives the non-linear elemental stiffness matrices. Since this matrix is a function of 1-D strain variables one has to repeat the process till it converges. Using these converged 1-D strain vector or 1-D generalized strains, find the final non-linear elemental stiffness matrices and again run 1-D code to get all final 1-D responses.

The dynamic response of non-linear, flexible multi-body systems is simulated within the framework of energy-preserving and energy-decaying time integration schemes that provide unconditional stability for non-linear systems. The kinematic description of bodies and joints in their undeformed and deformed configurations are make use of three orthogonal triads. First, an inertial triad, S_I , is used as a global reference for the system with unit vectors \bar{i}_1, \bar{i}_2 , and \bar{i}_3 . A second triad, S_0 , is attached to the body and defines its orientation in the reference configuration with unit vectors $\bar{e}_{01}, \bar{e}_{02}$, and \bar{e}_{03} . Finally, a third triad, S^* , defines the orientation of the body in its deformed configuration with unit

vectors \underline{e}_1 , \underline{e}_2 , and \underline{e}_3 . The kinetic and strain energies of the beam are

$$\mathcal{K} = \frac{1}{2} \int_0^L \underline{v}^{*T} M^* \underline{v}^* dx_1; \quad \mathcal{V} = \frac{1}{2} \int_0^L \underline{e}^{*T} C^* \underline{e}^* dx_1 \quad (9)$$

respectively. Where L is the length of the beam; x_1 is the curvilinear coordinate along the reference line; M^* and C^* are the components of the sectional inertial and stiffness tensors respectively; and \underline{v}^* and \underline{e}^* are the components of the sectional velocity and strain vectors respectively. The superscript $(\bullet)^*$ is used to denote tensor components measured in its deformed configuration. The equations of motion of the beam from Hamilton's principle is as follows:

$$\int_{t_i}^{t_f} \int_0^L (\delta \underline{v}^{*T} M^* \underline{v}^* - \delta \underline{e}^{*T} C^* \underline{e}^* + \delta \mathcal{W}^a) dx_1 dt = 0 \quad (10)$$

where $\delta \underline{v}^{*T}$ and $\delta \underline{e}^{*T}$ are virtual variations in sectional velocities and strains, respectively, $\delta \mathcal{W}^a$ is the virtual work done by the externally applied forces. The final form of equations of motion of the beam are as follows:

$$\begin{aligned} (\mathcal{R} \mathcal{R}_0 \underline{p}^*)' + \mathcal{U} [\tilde{u}] \mathcal{R} \mathcal{R}_0 \underline{p}^* - (\mathcal{R} \mathcal{R}_0 \underline{f}^*)' \\ - \mathcal{U} [\tilde{u}'_0 + \tilde{u}'_l] \mathcal{R} \mathcal{R}_0 \underline{f}^* = \underline{q} \end{aligned} \quad (11)$$

where the sectional momenta and elastic forces are defined as $\underline{p}^* = M^* \underline{v}^*$ and $\underline{f}^* = C^* \underline{e}^*$ respectively; and \underline{q} are the external forces. An energy-preserving discretization of these equations of motion Eq. (11) is performed. The inertial and elastic forces are discretized to yield the following discretized equations of motion

$$\begin{aligned} \frac{\mathcal{R}_f \mathcal{R}_0 \underline{p}_f^* - \mathcal{R}_i \mathcal{R}_0 \underline{p}_i^*}{\Delta t} + \mathcal{U} \left[\frac{\tilde{u}_f - \tilde{u}_i}{\Delta t} \right] \mathcal{R}_a \mathcal{R}_0 \frac{\underline{p}_f^* + \underline{p}_i^*}{2} \\ - (\mathcal{R}_b \mathcal{R}_0 \underline{f}_m^*)' - \mathcal{U} [\tilde{u}'_0 + \tilde{u}'_m] \mathcal{R}_b \mathcal{R}_0 \underline{f}_m^* = \underline{q}_m \end{aligned} \quad (12)$$

where $(\bullet)_m = ((\bullet)_f + (\bullet)_i)/2$; and all the rotation operators and the discretization of finite rotations are defined in Appendix A & B of [4].

In the formulation of flexible joint elements, the strain energy in the flexible joint is defined as follows:

$$\mathcal{V} = \frac{1}{2} \underline{s}^{*T} C^* \underline{s}^* \quad (13)$$

where C^* are the components of the flexible joint stiffness tensor and \underline{s} , inducing deformations in the flexible joint in terms of relative displacements ($\underline{u} = \underline{u}^k - \underline{u}^l$) and relative rotations ($\delta \underline{\psi} = \delta \underline{\psi}^k - \delta \underline{\psi}^l$) of the two bodies $(\bullet)^k$ and $(\bullet)^l$. The energy-preserving formulation for flexible joints consists of the elastic force discretization together with the following constitutive laws:

$$\underline{f}_m^* = C^* (\underline{s}_f^* + \underline{s}_i^*)/2 \quad (14)$$

In the formulation of constraint elements, for the case of revolute joint elements, using the properties of the revolute joint develop all kinematic constraints. The following two

kinematic constraints in the deformed configuration are defined as follows from the condition of no relative displacements are allowed.

$$C_1 = g_{31} = \underline{e}_3^{kT} \underline{e}_1^l = 0 \quad (15)$$

$$C_2 = g_{32} = \underline{e}_3^{kT} \underline{e}_2^l = 0 \quad (16)$$

The third constraint obtained from the definition of the relative rotation ϕ between the two bodies is defined as follows:

$$C_3 = g_{11} \sin \phi + g_{12} \cos \phi = 0 \quad (17)$$

where $g_{11} = \underline{e}_1^{kT} \underline{e}_1^l$ and $g_{12} = \underline{e}_1^{kT} \underline{e}_2^l$; and the components of vector $(\vec{\bullet})$ measured in S_I and S^* denoted by (\bullet) and $(\bullet)^*$, respectively.

3 3-D Recovery Analysis

To recover 3-D results at a specific section, one need to provide additional information obtained from the 1-D global beam analysis along with 2-D warping & strain recovery relations, a bi-product of 2-D cross-sectional analysis. One can carry out 3-D recovery based on the classical model or the generalized Timoshenko model or the generalized Vlasov model. The input given is different from model to model.

4 Numerical Example(s)

4.1 The four bar mechanism problem

The numerical example deals with a four bar mechanism problem depicted in Fig. (2). Bar 1 is of length $L_1 = 0.12$ m and is connected to the ground at point A by means of a revolute joint. Bar 2 is of length $L_2 = 0.24$ m and is connected to bar 1 at point B with a revolute joint. Finally, bar 3 is of length $L_3 = 0.12$ m and is connected to bar 2 and the ground at points C and D, respectively, by means of two revolute joints. In the reference configuration the bars of this planar mechanism intersect each other at 90^0 angles and the axes of rotation of the revolute joints at points A, B, and D are normal to the plane of the mechanism. However, the axis of rotation of the revolute joint at point C is at a 5^0 angle with respect to this normal to simulate an initial defect in the mechanism. A torque is applied on bar 1 at point A so as to enforce a constant angular velocity $\Omega = 20$ rad/sec. If the bars were infinitely rigid, no motion would be possible as the mechanism locks. For elastic bars, motion becomes possible, but generates large internal forces. The physical characteristics of the three bars are tabulated in Table 1.

The Saint-Venant torsion constant J is calculated from the following equation.

$$J = \frac{ba^3}{3} - \frac{64a^4}{\pi^5} \sum_{n=0}^{\infty} \frac{\tanh(\frac{knb}{2a})}{(2n+1)^5} \quad (b \geq a) \quad (18)$$

where $k_n = \frac{(2n+1)\pi}{a}$ and b, a are the cross-sectional dimensions along x_2, x_3 directions, respectively. The approximate

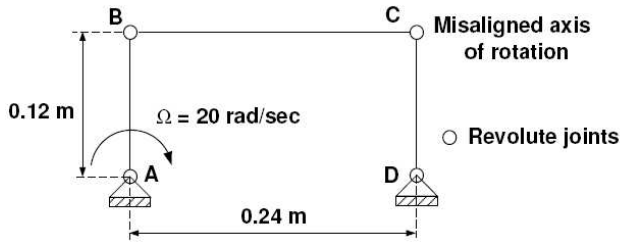


Figure 2: The four bar mechanism problem

Table 1: The physical characteristics of the three bars of the four bar mechanism

Bar 1:	
Axial stiffness:	$EA = 40 \text{ MN}$
Bending stiffnesses:	$EI_{22} = EI_{33} = 0.24 \text{ MN.m}^2$
Torsional stiffness:	$GJ = 0.28 \text{ MN.m}^2$
Mass per unit span:	$m = 3.2 \text{ kg/m}$
Bars 2 & 3:	
Axial stiffness:	$EA = 40 \text{ MN}$
Bending stiffnesses:	$EI_{22} = EI_{33} = 24 \text{ kN.m}^2$
Torsional stiffness:	$GJ = 28 \text{ kN.m}^2$
Mass per unit span:	$m = 1.6 \text{ kg/m}$

value of J can be found from the following expression.

$$J \approx 2.249232 a^4 \quad \text{for } (2a \times 2a) \quad (19)$$

The calculated values are tabulated in Table 2, which are used for cross-sectional analysis. Each cross-section of

Table 2: The calculated values for cross-sectional analysis

Bar 1:	
Cross-section:	$(0.26833 \text{ m} \times 0.26833 \text{ m})$
Young's modulus:	$E = 555.55556 \times 10^6 \text{ N.m}^2$
Poisson's ratio:	$\nu = -0.28$
Mass density:	$\rho = 44.44444 \text{ kg/m}^3$
Bars 2 & 3:	
Cross-section:	$(0.08485 \text{ m} \times 0.08485 \text{ m})$
Young's modulus:	$E = 5555.55556 \times 10^6 \text{ N.m}^2$
Poisson's ratio:	$\nu = -0.28$
Mass density:	$\rho = 222.2222 \text{ kg/m}^3$

bar 1, 2, and 3 is divided into 100, eight-node isoparametric finite elements. The stiffness and mass matrices obtained from the linear cross-sectional analysis of bar 1, 2, and 3 are given in the Appendix D. The beam 1 and beam 3 reference line is divided into 2-equal elements each and the beam 2 reference line is divided into 4-equal elements for 1-D non-linear analysis. For this four bar mechanism problem, the automated time step size procedure is used. The desired local error level is set to be $\hat{\epsilon} = 1.0 \times 10^{-06}$ and a new time step size is evaluated at each time step [16].

This problem is simulated for a total of 0.5 sec using the energy-decaying scheme. If the four revolute joints had their axes of rotation orthogonal to the plane of the mechanism, the response of the system would be purely planar, and bars 1 and 3 would rotate at constant angular velocities around points A and D, respectively. The initial defect in the mechanism causes a markedly different response. Figure (3) shows the time history of the relative rotations at points A and D, as well as the absolute rotation of the mid-point of bar 2. Bar 1 rotates at a constant angular velocity under the effect of the applied torque, but bar 3 now oscillates back and forth, never completing an entire turn. When the direction of rotation of bar 3 reverses, bar 2 undergoes large rotations, instead of near translation. Furthermore, the response is three-dimensional as shown in Fig. (4) which depicts the time history of out-of-plane displacements at points B and C. Point C undergoes a 3 mm maximum out-of-plane displacement. The time history of the three components of the internal force at the root of bar 1 are shown in Fig. (5), whereas Fig. (6) shows the time history of components of twisting and bending moments at the same location. The corresponding quantities at mid-span of bar 2 are shown Figs. (7) and (8). These large internal forces are all caused by the initial imperfection of the mechanism.

The large coupling terms in the final non-linear stiffness matrix of each beam are responsible for large variation in the non-linear 3-D responses. Figure (9) shows the 3-D plot of extension-twist coupling coefficient, S_{14}^{NL} , of the non-linear stiffness matrix variation of bar 1. Figure (13) shows the 3-D plot of 1-D strain vector component, κ_1 , of bar 1. Figure (10) shows the 3-D plot of extension-bending in 2-direction coupling coefficient, S_{15}^{NL} , of the non-linear stiffness matrix variation of bar 1. Figure (14) shows the 3-D plot of 1-D strain vector component, κ_2 , of bar 1. Figure (11) shows the 3-D plot of extension-bending in 3-direction coupling coefficient, S_{16}^{NL} , of the non-linear stiffness matrix variation of bar 1. Figure (15) shows the 3-D plot of 1-D strain vector component, κ_3 , of bar 1. From these figures, one can observe that S_{15}^{NL} is dominant with maximum positive value 60,000 followed by S_{14}^{NL} with 25,000 and these both terms negative magnitude is same and equal to 10,000. But S_{16}^{NL} both positive negative magnitude equal to 4,000. So, the elastic bending curvature in 2-direction, κ_2 , is more with magnitude 0.07 followed by the elastic twist, κ_1 , with magnitude 0.03 of bar 1 and the elastic bending curvature in 3-direction, κ_3 , is very less with magnitude equal to 0.005. The extension of the reference line of bar 1, γ_{11} , with magnitude equal to 0.0002, which is negligible. Thus, with the applied torque on bar 1 there is no significant amount of extension of bar 1. But in the case of bar 2, S_{14}^{NL} and S_{15}^{NL} are equally significant compared to the third term. Similar conclusions can be made as above from Figs. ((12) and (16); (17) and (21); (18) and (22)) for bar 2. But in the case of bar 3, S_{15}^{NL} is more significant compared to other two terms. Similar conclusions can be made as above from Figs. ((19) and (23); (20) and (24); (25) and (29)) for bar 3. Figures (26), (27) and (28) shows the 3-D plot of 1-D strain vector component variation of bar 1, 2, and 3, respec-

tively for linear and non-linear cases. As expected there is no significant extension of the reference line of all bars. Note that Figs. (17) to (29) are not included because of space limitation.

It has been observed [17] that the two schemes (EPS & EDS) are in very close agreement, and yield smooth time history responses for all quantities. The prediction of the velocities at point *C*, and the quarter-point forces in bar 1 using EPS are presented. These results shows that very high frequency oscillations of a purely numerical origin are present in the predictions of the EPS. The high frequency numerical dissipation featured by the EDS completely eliminates this undesirable numerical noise.

5 Conclusions

The results for the four-bar mechanism problem shows that the dynamic responses for linear and non-linear analyses are not deviating much because of not having strong coupling terms in the final non-linear stiffness matrices. This is because of the square cross-section for all three bars in the mechanism. It has been observed that as the cross-section departs from a strip configuration, the trapeze effect becomes less and less important compared to the overall torsional rigidity. Using strip-beam analysis, one can see the large variation in the linear and non-linear dynamic responses as compared to the problem analyzing with trapeze effect and will be addressed in future work. In the present four-bar mechanism problem, cross-sectional nonlinearities are small eventhough 1-D nonlinearities are large. There is no convergence difference is observed. However, when cross-sectional nonlinearities are also become important, then convergence might be an issue and is currently being studied. In the present problem, the 1-D generalized strain vector converges after 8 iterations. Results obtained & presented for linear case are using multi-body dynamics software DYMORE.

References

- [1] D. A. Danielson, and D. H. Hodges, "Nonlinear beam kinematics by decomposition of the rotation tensor," *Journal of Applied Mechanics*, Vol. 54, 1987, pp. 258–262.
- [2] D. H. Hodges, "A review of composite rotor blade modeling," *AIAA Journal*, Vol. 28, 1990, pp. 561–565.
- [3] V. L. Berdichevsky, "Variational-asymptotic method of constructing a theory of shells," *Prikladnaya Matematika i Mekhanika (PMM)*, Vol. 43, 1979, pp. 644–687.
- [4] C. E. S. Cesnik, and D. H. Hodges, "VABS: a new concept for composite rotor blade cross-sectional modeling," *Journal of the American Helicopter Society*, Vol. 42, 1997, pp. 27–38.
- [5] W. Yu, "Variational Asymptotic Modeling of Composite Dimensionally Reducible Structures," *PhD Thesis, Aerospace Engineering, Georgia Institute of Technology, Georgia, USA, May, 2002.*
- [6] C. E. S. Cesnik, D. H. Hodges, B. Popescu, and D. Harursampath, "Composite beams cross-sectional modeling including obliqueness and trapeze effects", *Proc. 37th Structural Dynamics and Materials Conference*, pp. 1384–1397. *AIAA Paper 96-1469.*
- [7] D. H. Hodges, D. Harursampath, V. V. Volovoi, and C. E. S. Cesnik, "Non-classical effects in non-linear analysis of pretwisted anisotropic strips," *International Journal of Non-Linear Mechanics*, Vol. 34, 1999, pp. 259–277.
- [8] D. Harursampath, "Non-Classical Non-Linear Effects in Thin-Walled Composite Beams," *PhD Thesis, Aerospace Engineering, Georgia Institute of Technology, Georgia, USA, December, 1998.*
- [9] K. L. Frank (ed.), *Nonlinear Composite Beam Theory, Vol. 213 of PROGRESS IN ASTRONAUTICS AND AERONAUTICS*, American Institute of Aeronautics and Astronautics, Inc., 1801 Alexander Bell Drive, Reston, Virginia 20191-4344. See also URL <http://www.aiaa.org>.
- [10] O. A. Bauchau, and N. K. Kang, "A multi-body formulation for helicopter structural dynamic analysis," *Journal of the American Helicopter Society*, Vol. 38, 1993, pp. 3–14.
- [11] O. A. Bauchau, "Computational schemes for flexible, nonlinear multi-body systems," *Multibody System Dynamics*, Vol. 2, 1998, pp. 169–225.
- [12] O. A. Bauchau, and D. H. Hodges, "Analysis of nonlinear multi-body systems with elastic couplings," *Multibody System Dynamics*, Vol. 4, 1999, pp. 168–188.
- [13] W. Yu, "An integrated approach for efficient high-fidelity analysis of composite structures", *Proc. 46th AIAA/ASME/ASCE/AHS/ASC Structures, Structural Dynamics and Materials Conference, AIAA-2005-1911.*
- [14] E. A. Armanios, A. Makeev, and D. Hooke, "Finite displacement analysis of laminated composite strips with extension-twist coupling," *Journal of Aerospace Engineering*, Vol. 9, 1996, pp. 80–91.
- [15] B. Popescu, and D. H. Hodges, "Asymptotic treatment of the trapeze effect in finite element cross-sectional analysis of composite beams," *International Journal of Non-Linear Mechanics*, Vol. 34, 1999, pp. 709–721.
- [16] B. Popescu, "Asymptotically Correct Refinements in Numerical Cross-Sectional Analysis of Composite Beams," *PhD Thesis, Aerospace Engineering, Georgia Institute of Technology, Georgia, USA, June, 1998.*
- [17] O. A. Bauchau, and C. L. Bottasso, "On the Design of Energy Preserving and Decaying Schemes for Flexible, Nonlinear Multi-Body Systems," *Computer Methods in Applied Mechanics and Engineering*, Vol. 169, 1999, pp. 61–79.

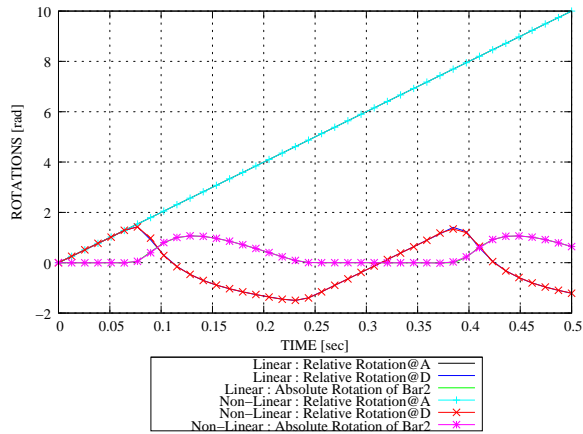


Figure 3: Time history of rotations of the system.

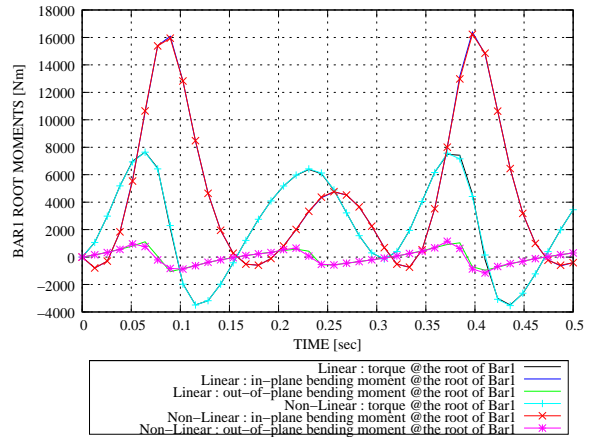


Figure 6: Time history of moments at the root of Bar 1, in local axes.

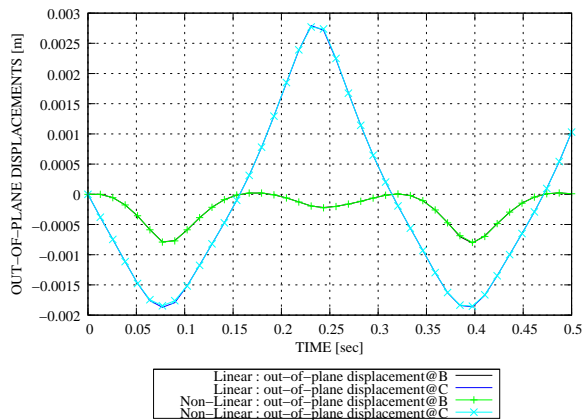


Figure 4: Time history of out-of-plane displacements at points B and C.

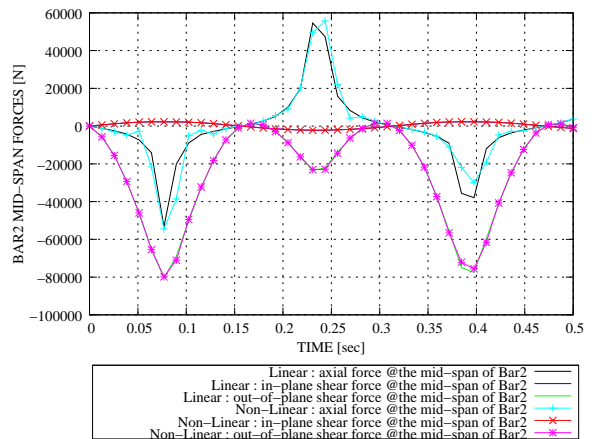


Figure 7: Time history of forces at mid-span of Bar 2, in local axes.

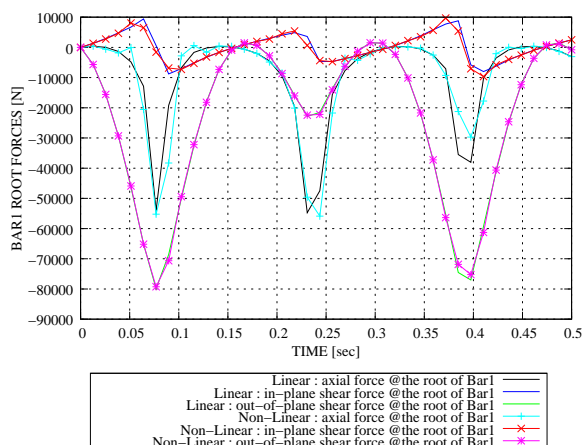


Figure 5: Time history of forces at the root of Bar 1, in local axes.

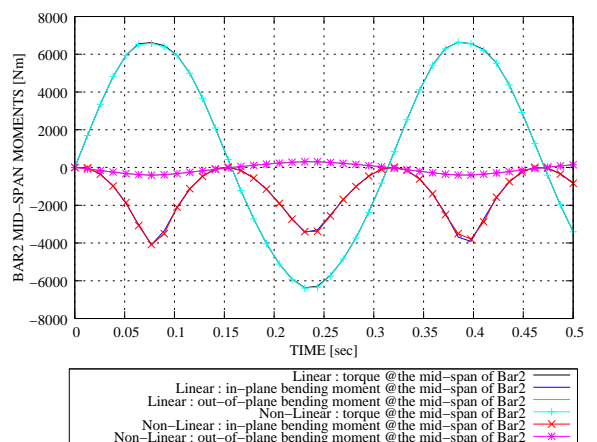


Figure 8: Time history of moments at mid-span of Bar 2, in local axes.

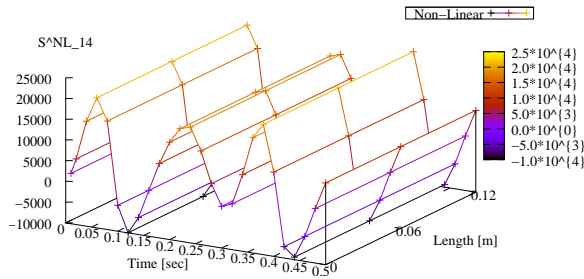


Figure 9: 3-D plot of extension-twist coupling coefficient of the non-linear stiffness matrix variation of Bar 1.

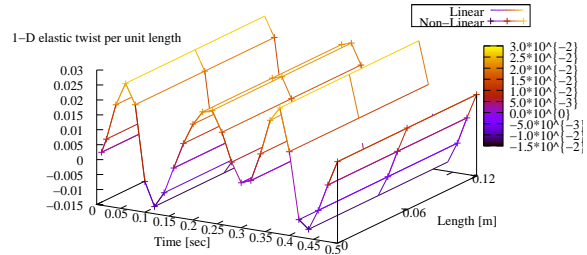


Figure 13: 3-D plot of 1-D strain vector component variation of Bar 1.

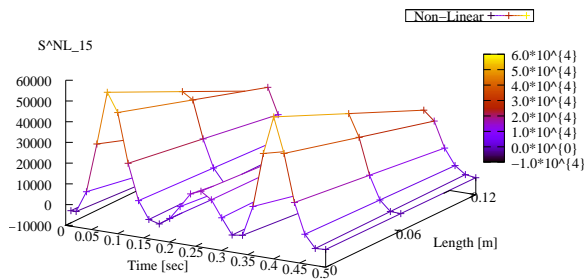


Figure 10: 3-D plot of extension-bending in 2-direction coupling coefficient of the non-linear stiffness matrix variation of Bar 1.

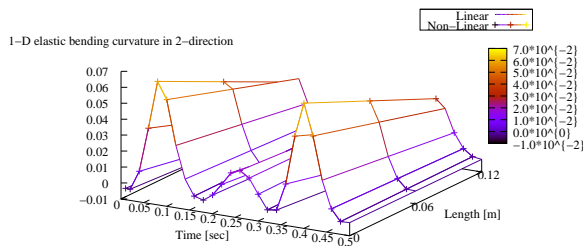


Figure 14: 3-D plot of 1-D strain vector component variation of Bar 1.

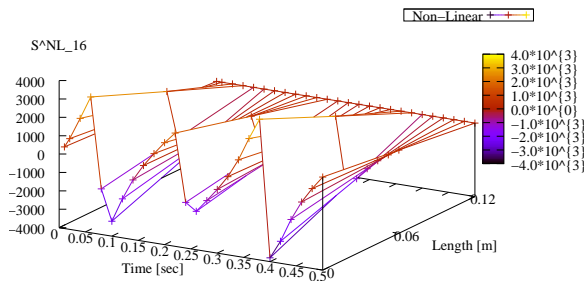


Figure 11: 3-D plot of extension-bending in 3-direction coupling coefficient of the non-linear stiffness matrix variation of Bar 1.

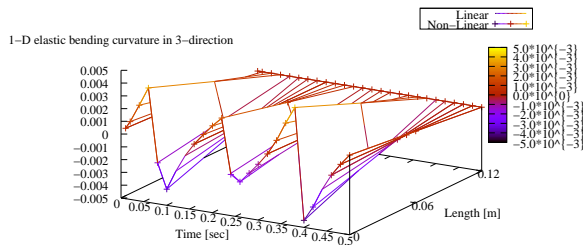


Figure 15: 3-D plot of 1-D strain vector component variation of Bar 1.

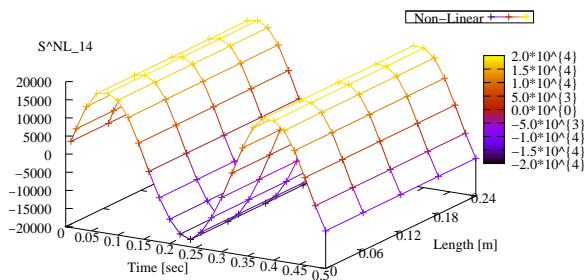


Figure 12: 3-D plot of extension-twist coupling coefficient of the non-linear stiffness matrix variation of Bar 2.

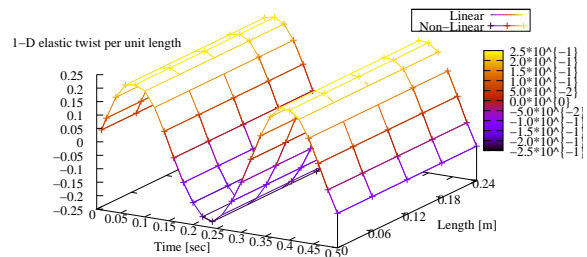


Figure 16: 3-D plot of 1-D strain vector component variation of Bar 2.